AD-A145 682 TOMOGRAPHIC RECONSTRUCTION OF NEUTRON RADIOGRAPH IMAGES 1/1
(U) LOCKHEED MISSILES AND SPACE CO INC SUNNYVALE CA
S M JAFFEY ET AL. 11984 LMSC-D-966339 N00014-81-C-2227

UNCLASSIFIED F/G 20/6 NL

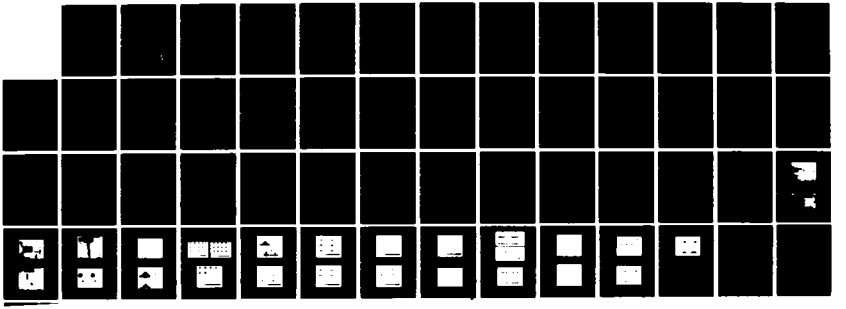

END

FILMED

DTIC

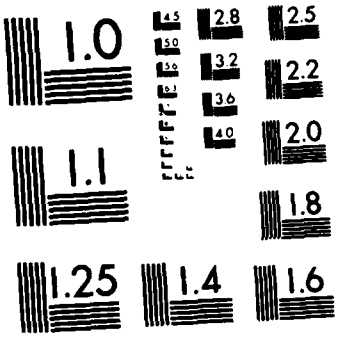

TOMOGRAPHIC RECONSTRUCTION OF NEUTRON RADIOGRAPH IMAGES

FINAL TECHNICAL REPORT

Lockheed Missiles & Space Company, Inc.
SUNNYVALE, CALIFORNIA

1984

TOMOGRAPHIC RECONSTRUCTION OF NEUTRON RADIOGRAPH IMAGES

FINAL TECHNICAL REPORT

Stephen M. Jaffey
Kalyan Dutta

NRL Contract N00014-81-C-2227

Submitted by

LOCKHEED MISSILES & SPACE COMPANY, INC.
Palo Alto Research Laboratories

TABLE OF CONTENTS

SECTION 1

OVERVIEW AND SUMMARY

1.

This report covers an investigation of the application of computer-aided tomography to the problem of nondestructive inspection of industrial components. The work presented here describes the application of tomographic techniques to neutron radiography. A comparison of neutron and x-ray tomography is included. Additionally, the capability for three-dimensional visualization of inspection data, made possible by the use of tomographic methods, is described.

This work was initiated by Dr. J. Blodgett of the Naval Research Laboratory for the Materials Division of the Naval Air Systems Command. Of particular interest were the possibilities tomography offered of increased contrast sensitivity and 3D visualization during field inspection of aircraft components.

1.1. Introduction

At the present time, x-ray projection radiography is a widely used nondestructive testing (NDT) technique in industrial inspection. In recent years, an x-ray imaging technique called computer-aided tomography (CT) has been very successful in providing cross-sectional images of the internal structure of three-dimensional objects. CT has had a major impact in medical imaging, where it has provided improved visibility of low-contrast lesions and tumors that could not be seen in projection radiographs.

Because of the costs currently associated with the acquisition of image data and computer-aided reconstruction of cross-sectional images, the major advances in CT techniques have primarily been in medical imaging. However, with the increasing availability of cheaper, improved radiation sources and detectors, and with improvements in general-purpose tomographic reconstruction software, CT techniques are increasingly applicable to NDT inspection tasks.

In some respects tomographic techniques are more applicable to industrial inspection than to medical imaging. Unlike the situation in medical imaging where there are biological limits to the dosage that may be used and where rapid data acquisition and near on-line processing of the data is desirable, in industrial NDT situations the required data can be obtained on film or other detectors using optimum levels of radiation dosage and exposure times, and scanned and converted to digital imagery to be

processed later. For these reasons CT techniques are now very appropriate for NDT inspection.

1.2. Relationship of Neutron CT to Other CT Techniques

We applied the mathematics of tomographic reconstruction from projections to neutron radiographs. This mathematics and associated algorithms have been well developed for medical CT. Although neutron and x-ray attenuation mechanisms differ, the same attenuation equation and thus reconstruction mathematics and algorithms apply.

In comparison with medical CT, industrial x-ray CT is a new but rapidly developing field. Several companies are developing prototype industrial machines and at least two are renting time on their machines and/or selling commercial models. We purchased x-ray computed tomograms for comparison with the neutron tomograms of the same test sample.

Neutron tomography has been little explored. The only known work prior to or concomitant with this project has been the application of high energy reactor neutrons to reconstruction of nuclear fuel rod bundles [Barton,1977; Schlapper,1980; Richards,1982; de Volpi,1982] and biological tissues [Koeppe,1981]. Industrial inspection applications of neutron radiography generally use thermal neutrons due to higher obtainable neutron flux. Our project focused on the use of thermal neutrons for non-destructive inspection of an aircraft component, keeping in mind the adaptation to mobile thermal neutron sources.

The utility of neutron-beam computed tomography will be in the increased contrast sensitivity over neutron and x-ray radiography, and x-ray CT for materials contrasted better by neutrons than x-rays.

1.3. Objectives

The major objective of this study was to develop a system for the tomographic reconstruction of images obtained from a neutron-beam imaging experiment. While the reconstruction of x-ray projection data is commonly done, neutron-beam tomographic reconstructions have not yet been investigated as an inspection tool.

A second objective of this study was to obtain x-ray tomograms of the same inspection part that was used in the neutron-beam experiment, in order to compare the relative qualities of x-ray and n-beam tomographic reconstructions.

The tomographic reconstructions were performed on a test specimen especially fabricated for the purpose. It consisted of a fragment of an aircraft fuselage that includes several structural members (including fasteners, rivets, etc.), and also a second section composed of several calibrated phantoms (titanium, steel and aluminum cylinders).

Photographs of this specimen are shown in Figures 1 and 2 (at the end of the text section of this report).

Unlike the case of x-ray tomography, no special-purpose

scanners exist for n-beam tomography, and thus the preliminary experiments described here, done using an unoptimized radiation source and a manually rotated specimen stage, give results that can be much improved with equipment designed for the purpose.

1.4. Proposed Tasks

The study had the following basic tasks:

1) Determination of system requirements, and acquisition of a set of x-ray tomograms through a suitable industrial inspection component.

2) Generation of fast tomographic reconstruction software based on an array processor implementation of general-purpose reconstruction programs.

3) Tomographic reconstruction of several slices through the specimen, obtained from scanned and registered neutron-beam projection radiographs supplied by the Naval Research Laboratory.

4) A comparison of the techniques of x-ray and neutron tomography and of the results obtained from these techniques.

5) Development of a three-dimensional data base from these tomographic reconstructions, and application of the technique of "reprojection" to these data bases to obtain high contrast three-dimensional displays of structures of interest.

1.5. Summary

Section II briefly describes the concepts of computed tomography. Section III reports on our work in neutron computed tomography. Section IV describes the x-ray tomograms acquired on the same inspection part. It also compares the relative qualities obtainable from the x-ray and the n-beam methods. Section V describes three-dimensional image synthesis, using data obtained from these reconstructions, and employing recently developed "reprojection" techniques to obtain pseudo-projection images with enhanced feature visibility. Section VI recommends future work.

SECTION II

COMPUTED TOMOGRAPHY CONCEPTS

2.

2.1. Reconstruction Algorithm

Numerous authors have discussed tomographic reconstruction algorithms [Herman,1980;Macovski,1983;etc.]. The required inputs are planar sets of parallel or fan beam line integrals of linear attenuation coefficients taken with a fixed source-detector geometry at multiple angles as the object rotates about an axis perpendicular to the plane.

We used the convolution backprojection algorithm. It exploits the central section theorem. Suppose a planar function f(x,y) is projected by integration along parallel rays into a scalar function p(r). Let F(u,v) be the two dimensional Fourier transform of f(x,y). Then the Fourier transform P(w) of the projection p(r) is the restriction of F(u,v) to the line passing through the origin and perpendicular to the projection rays.

Thus, we can fill in F(u,v) by taking projections at many angles and taking their Fourier transforms.

In concept the inverse two-dimensional Fourier transform yields the reconstruction of f(x,y). For computational simplicity and accuracy the computation is restructured as a sequence of 1D operations (including convolution) on each projection function.

2.2. Reconstruction Resolution

Reconstruction resolution is fundamentally limited by the spatial bandwidth of the projection measurement system [Bracewell,1977]. Basically, the measurement bandwidth determines the projection bandwidth which by the central section theorem limits the reconstructed image Fourier spectrum. Finite source size is the main factor limiting the resolution in the the neutron tomograms. The 75 mm diameter object adjacent to the film cassette and an L/D ratio of 50 yield a resolution of about 1.5 mm. Since the geometric unsharpness of an object point varies with projection angle, the reconstruction impulse response will generally be assymmetric and spatially variant [Verly,1979]. Note that the resolution of the projection data parallel to the rotation axis defines an effective tomogram thickness and limits the resolution in that direction in a 3D stack of tomograms.

Geometric misalignments (radiograph misregistrations) are the other main cause of resolution loss.

Reconstruction resolution also depends on a low pass filter embedded in the 1D convolution kernel. This filter trades off noise averaging against further resolution loss. We used the mildly smoothing Shepp-Logan filter [Huesman,1977].

Sampling also affects resolution. Minimizing aliasing when sampling each projection optimizes resolution and minimizes certain streak artifacts [Joseph and Spital,1980]. Coarse angular sampling generates streak artifacts emanating radially and at some distance from high contrast structures [Joseph and Schulz,1980]. To avoid these streaks the minimum number of projection angles is:

$$Nmin = 2 (Pi) R (Vm) \qquad (2.1)$$

where R is the object radius and Vm is the maximum spatial frequency in the reconstructed image. Less views are acceptable in practice. In our experiment the 90 views yielded low level streaking.

2.3. Line Integral Estimates and Errors

The line integrals, A, of the linear attenuation coefficient are estimated using the fundamental attenuation relationship:

$$A = - \ln(I(a)/I(u)) \qquad (2.2)$$

where I(a) and I(u) are the neutron intensities reaching a point on the detector plane after attenuation (a) by the object and unattenuated (u) in the absence of the object. With film-screen

recording I(a) and I(u) are estimated from the film optical densities.

The reconstruction image quality depends on errors in estimating A. For neutron radiography the major error sources are gamma radiation in the primary beam, secondary radiation, detector non-linearities, finite source size, and statistical fluctuations in the detected image and in the detection process.

The logarithmic attenuation relationship causes non-linear and object dependent propagation of measurement errors.

$$A + dA = - \ln ((I(a) + dI(a)) / (I(u) + dI(u))) \qquad (2.3)$$
$$= A + \ln (1 + dI(a)/I(a)) - \ln (1 + dI(u)/I(u))$$

The second order and higher terms of the systemmatic errors usually coherently degrade wide regions of the reconstructed images.

Detector non-linearity and secondary radiation were the primary problems for our CT reconstructions (Section 3.3). Gamma radiation in the primary beam, finite source size, and Poisson statistics may become significant errors when a mobile neutron source is used (Section 3.5).

SECTION III

NEUTRON-BEAM TOMOGRAPHY

3.

Neutron CT combines the contrast sensitivity and three-dimensional information of CT with the radiographic properties of neutrons. The latter includes contrasting of materials with similar densities, high contrast imaging of hydrogenous materials, and penetration of large thicknesses of some dense metals.

3.1. Underlying Physical Interactions

The information bearing image is formed by 70 kev electrons emitted by the gadolinium conversion screen after absorption of neutrons that have passed through the object without interacting. Several obfuscatory images increase the exposure. These arise from scattered neutrons and prompt emission of gamma rays following neutron capture by the object and the conversion screen. Gamma radiation in the primary beam adds additional degrading exposure. The dependence of the attenuation coefficients on neutron energy is quite small for thermal neutrons [Tyufakov,1979]

so that beam hardening, so troublesome in x-ray CT, is a minor problem in thermal neutron CT except for thick primarily absorbing materials.

3.2. Neutron Radiography

The neutron radiographs were recorded by Dr. Peter Moore of the Naval Research Laboratory at the National Bureau of Standards reactor, using a high purity filtered thermal neutron beam (1/40 eV). Exposures were recorded on type AA film using a 12.5 m vapor deposited gadolinium converter screen. One half minute exposures were taken to insure that film grain noise dominated the Poisson counting noise.

The test object was mounted on a stage (Figure 3) and manually rotated by 2 degrees between each of 90 exposures. To minimize effect of source size the stage was placed against the film cassette with the rotation axis 1.75" from the film plane. The rotation axis was aligned parallel to the film plane. The source to rotation axis distance was 73".

3.3. Digitization and Preprocessing

CT requires digital estimates of the line integrals of the linear attenuation coefficients along specific rays. Thus, the radiographs must be digitized, spatially registered and remapped in intensity.

3.3.1. Digitization

Each radiograph was imaged by a Sierra Scientific LSV 1.5" vidicon camera and digitized by a Lockheed improved Grinnel digitizer. Several steps were taken to ensure that TV resolution and electronic noise did not significantly degrade the radiographic information. Digitization was to 8 bit accuracy. 256 successive digitized frames of each radiograph were averaged. The spatial sampling interval of 0.35 mm was fine enough to avoid significant aliasing perpendicular to the rotation axis except for object points within an inch of the film. An analogue low pass filter reduced aliasing of the projection of nearby object points. Figures 4 and 5 show two digitized radiographs.

3.3.2. Registration

The radiographs were registered by linear resampling. Eight rectangular cadmium chips were attached to the neutron beam side of the film cassette for use as registration markers. Normalized cross-correlation was used to estimate the displacement of each marker with respect to one reference radiograph. For each image, the six coefficients of an affine transformation were estimated by a least squares fit to the eight fiducial mark displacements. Fit residuals were less than 0.2 mm in magnitude, indicating even smaller resulting misregistrations after resampling. Geometric distortion in the vidicon camera was less than 0.35 mm displacement across the field of view. These registration errors together with the finite source size limited the reconstruction resolution.

The CT algorithm requires samples recorded perpendicular to the axis of object rotation. To locate the axis, a #35 drill bit was attached to the rotation stage in coincidence with the rotation axis. Prior to registration, the digitized reference radiograph was rotated so that the rotation axis was parallel to image columns.

3.3.3. Spatial Averaging

The various effective computed tomography algorithms assume that the projection rays are all perpendicular to the object rotation axis. However, since the radiographs were recorded with a cone beam geometry, this assumption is invalid. To minimize artifacts from this effect, 5 adjacent rows in the digitized images were averaged prior to reconstruction. The resulting tomogram thickness is about 1.8 mm.

To facilitate array processor implementation parallel rather than fan beam geometry was assumed. The consequences should be small since the actual fan beam angle was only 2 degrees.

3.3.4. Line Integral Estimates

Line integrals, A, of the linear attenuation coefficient were estimated from Equation (2.2) assuming the film densities were proportional to the logarithm of the information bearing exposure. Analogue shading correction followed by logarithmic amplification resulted in digitized counts proportional to the film density.

The unattenuated intensity I(u) varied both spatially and between radiographs. Unfortunately, the specified object free calibration radiograph was not recorded. Therefore, estimates of the logarithm of I(u) were made by linear fits to the estimates of the logarithm of I(a) at points in each radiograph located outside of the projected image of the object.

3.3.5. Correction for Detector Non-linearity

Artifacts in the initial tomgrams of the calibrated cylinders (Figure 6a) resemble those due to non-linear detectors as described by Duerinckx [1979] for a pair of cylinders. In particular, the neutron tomograms exhibit broad dark and light streaks between cylinders and flaring out from cylinders. Moreover, a plot of image intensity versus position across the diameter of the steel cylinder shows the classic cupping artifact (Figure 7a). The non-linear detector model is the special case of Equation (2.3) when dA is a function of A.

One possible cause is non-linearity at the toe of the Hurter-Driffield curve. Unfortunately, the stepwedge included in the radiographs did not extend to the lowest density regions recorded for steel. A second possible cause of detector non-linearity is an approximately constant background bias due to secondary radiation from the object. Since neutron scatter [Barton,1983;de Volpi, 1983] and prompt emission gamma radiation [Newachek,1983] are both isotropically distributed, their intensity effect at the film plane has a low frequency spectrum that

falls off rapidly with object distance from the film plane [Stonestrom,1976; Robb,1983]. Both mechanisms would cause line integral underestimates that increased with increasing magnitude of the true line integral, an effect consistent with the sign of the image artifacts described.

We used a constant bias model to compensate for whichever or both of the effects were significant. This approach follows that suggested by Stonestrom [1976] and implemented by Joseph [1982]. The constant scattering level was simply varied until the artifacts were best suppressed as judged visually. Figure 6b shows the scatter corrected tomogram and Figure 7b the removal of the cupping artifact. The correction also reduced flares emanating from the highly attenuating structures in the fuselage fragment but introduced two low contrast streaks (Figure 8a,b).

After examining the radiographs Newacheck [1983] concluded that film non-linearity was the major effect. Furthermore, the background bias level of three tenths of the beam intensity through the titanium cylinder was considerably higher than that expected from crude neutron scatter calculations.

3.4. Evaluation of the Neutron Tomograms

The reconstructions were made using the convolution backprojection algorithm with the Shepp-Logan filter. Starting with a published software package [Huesman,1977], we implemented the rate limiting steps on a Floating Point Systems AP-120B array processor. The resulting 1 minute reconstruction times

facilitated interactive calibration experiments.

The reconstructions indicate the basic shapes, locations, and rough attenuation coefficients. They delineate structures unseen in the x-ray tomograms, but the resolution is poorer. Several reconstruction errors, or artifacts, are present. The main causes and potential corrections will be indicated.

3.4.1. Neutron Tomograms of Cylindrical Samples

Figure 9 shows 12 tomograms sampled at 1 mm spacing. The pixel width is 0.4 mm. Figure 10 shows x-ray tomograms for comparison (Section IV). The neutron reconstructions of the cylinder cluster faithfully capture the circular cross-sections and their locations. For example, vertical and horizontal measurements from the tomograms of the diameters of the three large cylinders agree to within 1 mm of the actual diameters. The steel, aluminum and titanium cylinders had diameters of .75", .5" and .375" respectively.

Diagonal cuts and fluted steel drill bits were placed in the cylinders to assess resolution. The diagonal cuts in the steel and titanium cylinders are faintly visible, but unseen in the aluminum. The spiral voids in the fluted steel bit embedded at the central axis of the steel cylinder are apparent but at much lower contrast than in the x-ray tomograms. The spiral steel bit is apparent as it rotates in the aluminum cylinder through the sequence of tomograms. However, the spiral voids are not apparent. All of these small features are better resolved in the

x-ray tomograms.

The discrepancy between indications of spiral voids in the steel but not the aluminum cylinder is unexplained. Note, however, that the contrast between void and cylinder is much lower for aluminum and that the voids lose considerable contrast due to limited reconstruction resolution.

The estimated linear attenuation coefficients sharply discriminate steel, titanium and aluminum, but err quantitatively in an object dependent manner.

3.4.2. Neutron Tomograms of Aircraft Fuselage Fragment

Figure 11 compares neutron and x-ray tomograms of the aircraft fuselage fragment. Figures 12, 13 and 14 show 16 neutron reconstructions sampled at 1 mm spacing through the fastener section. For comparison Figures 15, 16 and 17 show the corresponding x-ray tomograms (Section IV).

The image quality of the x-ray tomograms is better, but the neutron tomograms present many structures with superior contrast. The neutron tomograms have poorer resolution and various streak artifacts. These streaks are due to 4 missing or degraded projection radiographs, a slightly inadequate number of projection angles, and probably also to registration errors. In addition, parts of the fastener have somewhat poor definition probably due to residual uncorrected scatter or film non-linearities.

Better contrasting in the neutron tomograms is due as

expected to the properties of thermal neutron linear attenuation coefficients that make neutron radiography attractive for inspection purposes. The discrimination of materials with similar densities is illustrated by the reconstructed fastener. The x-ray tomogram shows the screw and nut with barely distinguishable densities, whereas the nut contrast sharply with the screw in the neutron tomograms. The highlighting of hydrogenous materials is exemplified for layers of rubber and epoxy. Even the paint around the stiffener shows up, although faintly, because the layer of paint is so thin.

3.5. Adaptation of Neutron Tomography to Mobile Sources

Because the NBS reactor neutron radiographs were of higher quality than is practical for mobile neutron sources, the Naval Research Laboratory requested that we discuss the problems mobile sources pose for neutron CT.

3.5.1. Low Neutron Beam Intensity

Usually CT cannot compensate for poor counting statistics. What it can do is increase contrast sensitivity by directly estimating the linear attenuation coefficients. Its efficient use of measurement geometry rather than of neutron counts enables this circumvention of the background trends characteristic of projection radiography. Note that the noise variance in a reconstructed CT image is approximately inversely proportional to the number of projection angles. Consequently, the exposure per

radiograph required to get tomograms with roughly the same noise levels as in a single radiograph is considerably less than for that single radiograph.

One exception where CT uses neutron statistics more efficiently is where multiple orientation views of the object are required. The same stack of CT slices can be reprojected from arbitrary orientations without new exposures. Projection radiography of course requires one exposure per viewpoint.

Computed tomography has specific constraints that reduce the fraction of detectable neutrons. Exposure time is lost during mechanical motion of the sample between measurements. A filmless video or solid state detection system would bypass cassette reloading time. Steps taken to minimize non-linear geometric artifacts by approximating pencil beam, pure neutron, scatter free imaging also degrade the efficiency of neutron intensity utilization. These steps can include source collimation, backscatter collimation grids, and dual measurement preprocessing (Section 3.5.3). In addition, increasing the source to object distance so that fan beams better approximate the cone beam will reduce available neutron beam intensity.

3.5.2. Effects of Low L/D Ratio

Because source size dominates the resolution, the average resolution cell width in the tomographic reconstructions varies approximately in inverse proportion to the L/D ratio and in proportion to the transverse radius of the object. Thus, for recon-

struction at a given resolution, the L/D ratio limits the object radius. An object with radius 75 mm imaged with an L/D of 15 will be reconstructed with resolution of about 3 to 4 mm.

Because the linear smearing effects of geometric unsharpness occur in the intensity domain prior to logarithmic processing (Equation 2.3), non-linear effects such as streaking [Stonestrom,1981] can arise near high contrast objects. Such non-linearities and associated artifacts may be significant especially since the geometric unsharpness would be worse than in medical CT and since industrial objects often have more high contrast edges than human bodies.

The remedy of a narrower collimator aperture costs in neutron intensity. Perhaps CT restoration [Bracewell,1977; Verly,1979] could reduce the artifacts and improve tomogram resolution. However, CT restoration is not well understood and would boost image noise levels thus requiring higher neutron exposures.

3.5.3. Effect of Gamma Ray Contamination of Projections

Mobile neutron source n-beams have varying levels of gamma radiation. In addition, prompt emission from object and conversion screen adds gamma exposure. However, direct exposure detection is mandated by speed requirements.

If reconstruction used the sum of intensities directly, then the tomograms would simply be weighted averages of pure neutron and gamma ray images. A loss of tomogram contrast would result in hydrogenous and other materials with high neutron attenuation

and low gamma ray attenuation. An additional contrast loss would result from prompt emission, and pair production. However, the logarithmic processing (Equation 2.3) introduces a non-linearity. One can speculate on the character of non-linear image artifacts by analogy to the well studied effect of beam-hardening in x-ray tomography.

The shared feature is two or more kinds of radiation for each of which the material attenuation coefficients are different. The multiple images superpose additively prior to logarithmic processing. Most x-ray sources have broad spectrums. The attenuation coefficients decrease with increasing photon energy causing the beam to 'harden' as it traverses the object. Beam hardening can cause streaks emanating from edges, flares surrounding objects, and streak artifacts between bones [Duerinckx,1979]. Note the similarity to non-linear detector artifacts.

The non-linearities and resultant artifacts for neutron-gamma ray imaging could be more severe because of the lack of correlation between neutron and gamma ray attenuation coefficients. The effect would be further complicated if the gamma ray contamination is broad spectrum and thus has its own beam hardening effects.

With dual measurements the gamma contamination could potentially be digitally removed before logarithmic processing. Macovski [1983] suggested simultaneous dual measurements for efficient use of exposure. For example, two pieces of film could

be placed together in front of a gadolinium foil in the back screen configuration. If the film adjacent to the foil has a single emulsion side facing the foil, then the low energy electrons emitted from the converter will expose primarily that emulsion. The gamma rays will expose both films.

The resulting two equations in two unknowns can be solved for the line integral, A(n), of the neutron attenuation coefficient and the total gamma ray contribution, I(g,k):

$$I(tot,k) = I(n,k) * \exp(-A(n)) + I(g,k) \qquad (3.1)$$

where I(n,k) is the detected neutron intensity in the absence of an object and I(tot,k) is the total neutron equivalent intensity detected by the kth piece of film.

This dual measurement scheme compensates for the background biases due to primary and secondary gamma radiation, except for some portion of the prompt emission gamma originating in the conversion screen. In addition, if collimation between the object and detector is used to remove primary beam gamma rays scattered from the object, then the dual measurement scheme might provide separate neutron and gamma ray tomograms in registration. As noted in Section 3.3.5 secondary gamma radiation from prompt emission object might also be dealt with by a constant background bias model.

SECTION IV

X-RAY TOMOGRAPHY, COMPARISON TO NEUTRON TOMOGRAPHY

4.

4.1. X-ray Tomograms

One original task was to acquire a multiangle x-ray radiographs and create tomograms from them. Shortly after we commenced the project, the first industrial x-ray CT became commercially available. Rather than duplicate work that others with more resources had achieved, we altered the task with the concurrence of Dr. Moore of NRL. The new task was to acquire x-ray tomograms on a commercial scanner. These tomograms would then be compared with our neutron tomograms in terms of image quality and complementary contrast sensitivity. They would also be used as a data base for making high contrast three-dimensional displays. The resources saved by this change were then applied to the remaining tasks.

For industrial inspection the medical tomography technology had to be modified to handle dense thick objects. Much higher

energy sources were required for object penetration. Detectors had to be developed for high energy low flux photon counting.

We had the test sample scanned and reconstructed on the Scientific Measurement Systems (SMS) industrial tomograph scanner in Austin, Texas [Hopkins,1981]. They used an isotopic 200 Curie (192)Ir source with energy concentrated at 310 keV (68%), 468 keV (23%), and 610 keV (3%). SMS uses an unique plastic scintillator detector system operated in the photon counting mode. These detectors are particularly efficient and inexpensive.

To attain tomograms suitable for three dimensional display and comparison with our neutron tomograms, we specified that SMS provide recontructions with constrast sensitivity of a few percent, their highest spatial resolution, and thin slice thickness. The detectors were fronted with lead collimators with apertures of 1.0 mm in width and 1.0 mm in height. The source was collimated with an exit aperture of 3.2 mm in width and 1.0 mm in height. In this configuration the reconstructions can resolve square wave patterned objects down to about 1.2 mm per line pair. SMS chose suitable sampling rates. They sampled each projection every 0.6 mm at 200 equally spaced angles.

Figure 10 shows tomograms of the cylinders. The six tomograms are sampled axially at 2 mm intervals. All of the cuts and the fluted drill bits are clearly revealed. The cylinders have quite uniform estimated linear attenuation coefficients (Figure 18). The low contrast circular artifacts are due to residual uncorrected x-ray scattering.

Figures 15, 16 and 17 show sixteen tomograms sampled at 1 mm intervals through the fuselage fragment. Contrast sensitivity in the display can be maximized by stretching the linear attenuation coefficients in the neighborhood of a particular material to fill the full 8 bit dynamic range of the refresh memory. Figure 19 shows a tomogram of the aircraft fuselage fragment with contrast settings centered around aluminum and steel.

4.2. Neutron Versus X-ray Tomography

For this study, the meaningful comparisons are between material contrast capabilities, underlying physical limitations, and available source strengths. As shown by the neutron tomograms, neutron tomography like neutron radiography can discriminate certain materials with similar densities and low density hydrogenous materials.

Scatter in high energy x-ray imaging is forward directed, and thus more difficult to eliminate or correct from a geometric point of view than the isotropic scattering for neutron imaging. Nonetheless, for some objects it may be desirable to separate the object and film cassette at the expense of resolution in order to reduce the frequency content of the scattered neutron background.

From an engineering viewpoint, higher equivalent intensity x-ray sources are available. For example, the industrial x-ray CT scanner at Aerojet Corporation (Sacramento, California) uses a linear accelerator and achieves 0.4 mm resolution in tomographic scans of 6" diameter objects recorded in under 20 minutes. Even

with the high intensity NBS reactor source used in our experiment, 45 minutes of exposures were required to achieve considerably less resolution for a smaller object. Mobile sources currently under development have considerably weaker sources necessitating image quality compromises such as low L/D ratio, and small source to object distances.

SECTION V

THREE-DIMENSIONAL DISPLAY BY REPROJECTION

5.

Currently there is considerable interest in three-dimensional visualization of a volume of interest for industrial inspection purposes. For example, we are concerned with the visualization of the three dimensional distribution of voids in the rocket motor chamber walls, as well as the internal configuration of nuclear fuel rod bundles. For aircraft component inspection, 3D display could potentially aid in visualizing the distribution, size, shape, and three 3D relationships of voids, cracks, inclusions, contaminants, and misaligned or missing parts. For example, knowledge of flaw orientation or the pattern of growth of a crack with time can be related to material strength.

Computed tomography yields very good two-dimensional image slices; for three-dimensional viewing, many such slices must be combined into a single view using a "reprojection" technique. Single views are necessary when the structure of interest crosses

between tomograms. It can be time consuming, unreliable, and sometimes impossible to visualize 3D structures simply by looking at a sequence of tomograms and mentally reconstructing the object. The idea is to use the full capabilities of the human visual system by presenting interactively modified dynamic, stereo projection views to the observer.

We have developed high speed reprojection algorithms and software under NSF Grant # ECS 79-25432 [Jaffey,1982;Dutta,1983] and Lockheed Independent Research Projects. We have applied the technique to the x-ray tomograms of the test specimen. Had time permitted, 3D display of contrasted structures such as rubber, paint, and bonding materials in the neutron tomograms would also have been informative. Discussions of the technique [Dutta,1983] and its application follow.

5.1. The Reprojection Technique

A reprojection operation consists of generating a two-dimensional view of a stack of CT slices, by suitably combining the linear attenuation coefficients in each slice along a given set of rays. The resulting images resemble ordinary radiographs. The great advantage of digital reprojection methods is that they allow processing of the CT data prior to reprojection so as to enhance the structures of interest by dissolving away unwanted regions or selective highlighting.

A reprojection algorithm computes the line integrals of the linear attenuation coefficient along a set of rays through a

volume of computed tomographic samples. Although these samples are discrete, the volume is considered to be filled by being modelled as a set of adjacent cubic volume elements (voxels) centered at each sample. Each voxel has uniform intensity equal to its estimated linear attenuation coefficient.

Each reprojection ray that intersects a particular voxel does so with an intersection length which we call a ray factor, or line length. The integrated linear attenuation coefficient along a ray is then obtained by suitably adding the product of the intensity and the ray factor for each voxel intersecting that ray.

5.2. Additive vs. Source-Attenuation Model for Reprojection

If the reprojected linear attenuation coefficient along a ray is obtained by simply adding together the ray factor contribution of each voxel, the resulting reprojection is called an additive model. In this case the voxel contributions may be computed in any order to obtain the final result.

In our more powerful source-attenuation model, each voxel acts both as a source contributing to the final density, and as an attenuator to reduce the contributions of other voxels along the ray that are farther from the observer. This is also a more general model, the additive model being obtainable from it by setting the attenuation coefficient to zero.

The observed ray intensity for the source-attenuation model

can be calculated in a recursive manner provided that the voxel contributions are calculated in an ordered way, from the farthest to the nearest voxel along the ray. At any stage only the net intensity need be retained. This results in a regular implementation very suitable for array processor mechanization.

The array processor implementation is particularly efficient for orthographic projections perpendicular to one of the three sampling axes. Our implementation was done on a Floating Point Systems AP120-B unit at the FORTRAN level.

5.3. Display of Fuselage Fragment

Several display experiments were done with the x-ray tomograms of the fuselage fragment. Figure 20 shows a rotating sequence of views reprojected additively from the original tomograms. The views resemble radiographs. Each adjacent pair of views is a stereo pair. Stereo viewing can provide good depth cues for this kind of imagery. When these views are successively displayed to a television monitor, the object appears to rotate, leading to depth perception from motion.

The power of reprojection lies in selective manipulations of the stack of tomograms prior to reprojection. For example, to increase the contrast of the fastener, all the tomogram pixels outside of the fastener were set to zero prior to reprojection (Figure 21). This zeroing was based on both location and amplitude. The resulting reprojections (Figure 22) have higher contrast than ordinary radiographs. They are analogous to x-rays of

the fastener alone, with the remainder of the object cut away.

In a second experiment the volume was dissected identically, but the source-attenuation reprojection model was used (Figure 23). The attenuation coefficients were set high so that only the nearest surfaces of the object are displayed. In this mode the reprojection performs hidden voxel removal. The intensity pattern in these views is unusual but does lead to excellent stereo fusion. We are currently working towards a more natural shading scheme for the nearest surfaces.

In a third experiment the sobel operator was used to enhance object edges and interfaces before reprojection (Figure 24). Figure 25 shows the resulting rotating additive reprojection sequence.

These examples illustrate the main features of reprojection display. Three-dimensional perception is achieved by stereo or motion or both. High contrast of selected structures is achieved by emphasis or dissection. Reprojection from any especially informative viewpoint is possible without collection of new data. We have implemented a variety of other volume operations including dynamic cutting, peeling away, and dissolving away. The accompanying video tape shows the dynamic form of these three-dimensional displays.

A work station with these display capabilities would give an inspector a powerful tool for visually manipulating a stack of tomograms. The aim is an interactive system for visualizing

three-dimensional structures of diagnostic significance that cross between tomograms and are not easily understood by viewing a sequence of individual tomograms.

SECTION VI

RECOMMENDATIONS FOR FUTURE WORK

6.

1) Determination of whether there are neutron radiography inspection applications for which the increased time requirement of neutron tomography could be justified by the increased contrast sensitivity that tomographic imaging provides.

2) Investigate the adaptation of neutron tomographic techniques to mobile accelerators.

- (A) Determine whether levels of background gamma will be high enough to necessitate correction. If so, investigate the dual measurement correction scheme.

- (B) Determine the severity of the non-linearity effects of low L/D ratio (around 15).

- (C) Investigate the use during reconstruction of apriori information about the scanned object in order to reduce the

required neutron exposures.

- (D) Investigate the use of a film free recording system with real-time digitization of the projection images to speed up the data acquisition.

3) If neutron tomography is judged useful, determine whether there is a subset of its applications that would benefit by three-dimensional visualization or analysis techniques. A digital work station designed for the interpretation of tomograms could be augmented with such display and analysis capabilities.

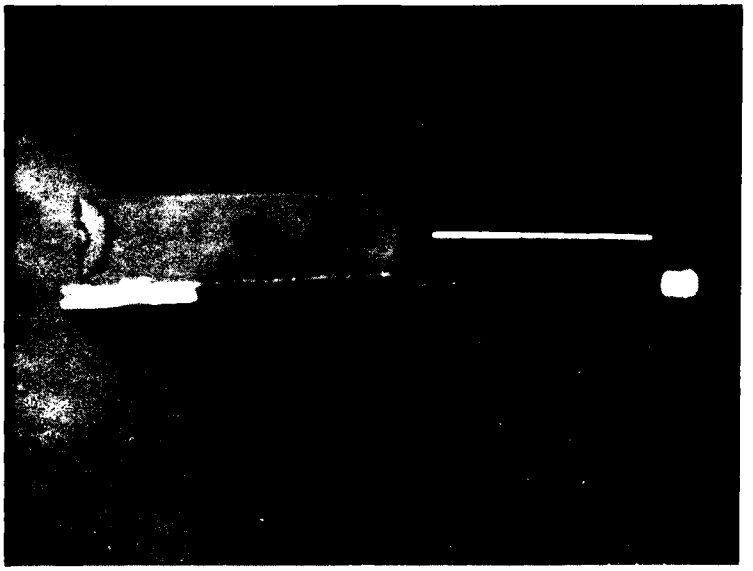

Figure 1
Photograph of the Test Specimen showing the aircraft fuselage fragment and the calibrated phantoms

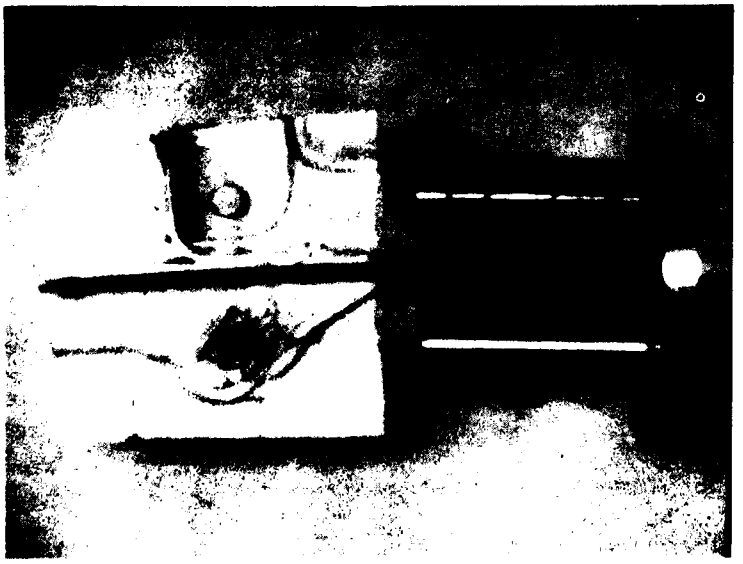

Figure 2
Photograph of the Test Specimen from another view angle

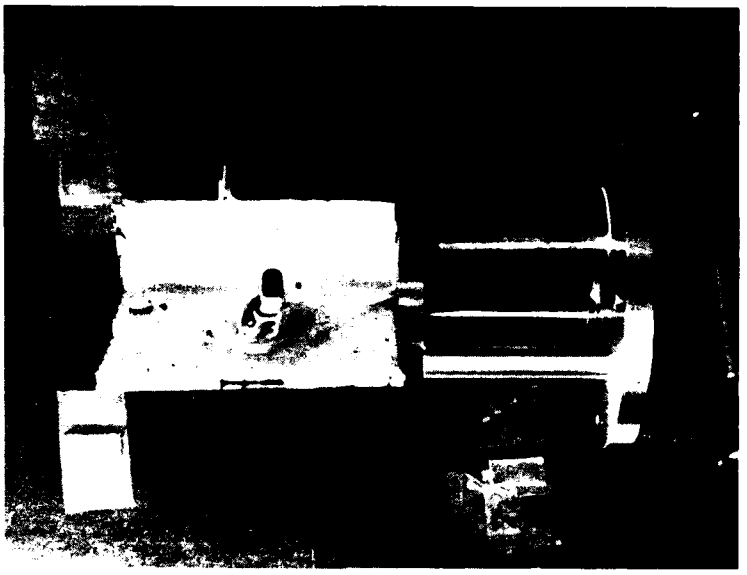

Figure 3
Photograph showing the Test Specimen, rotating stage and film cassette

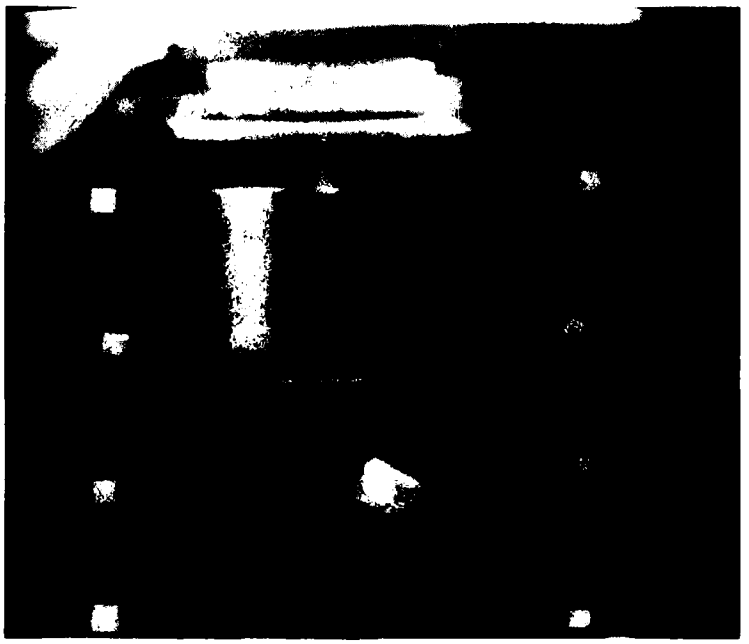

Figure 4
One of 90 digitized neutron radiograph images

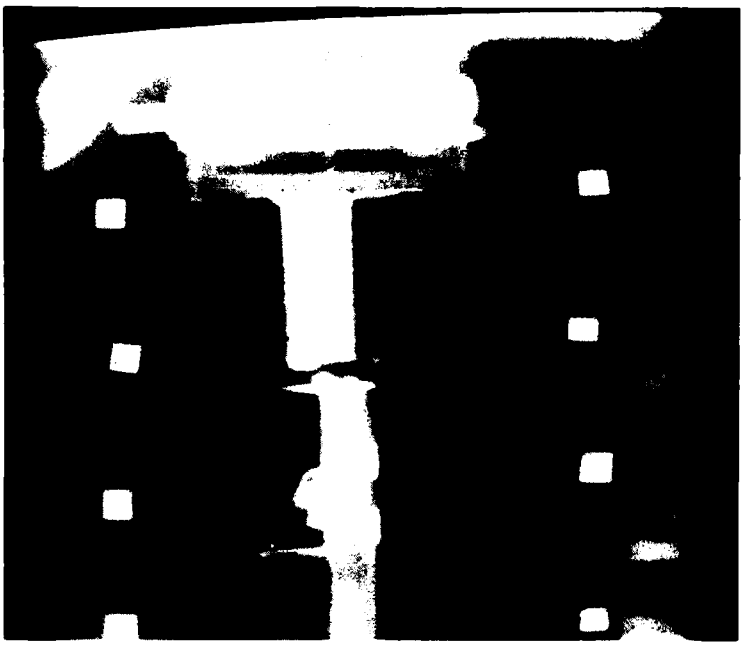

Figure 5
A second representative digitized neutron radiograph image

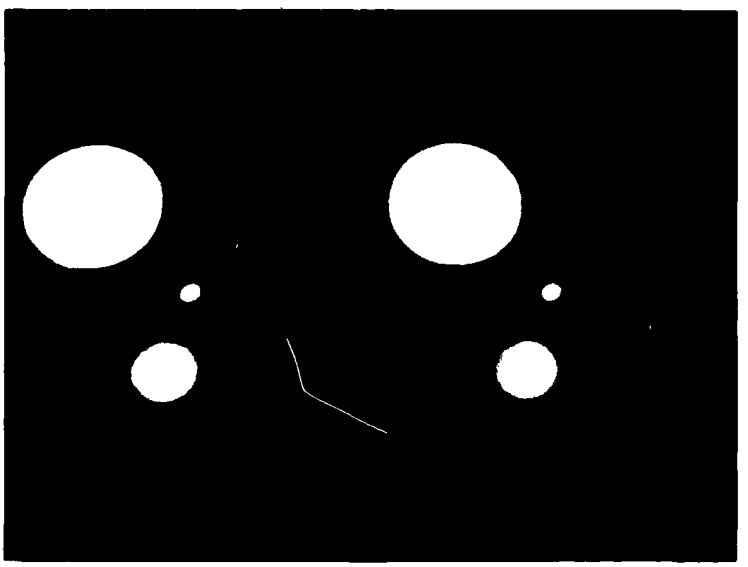

Figure 6
Reconstructed neutron tomograms showing effects of correction for scatter. Left: uncorrected, right: corrected for scatter

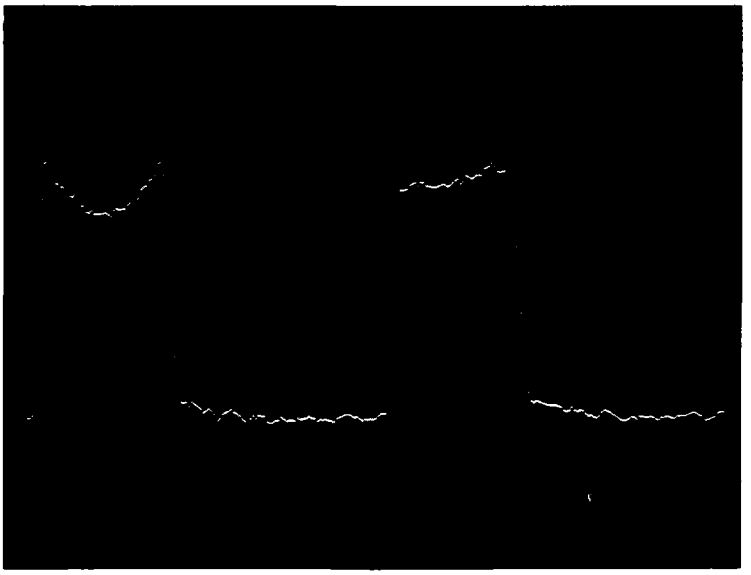

Figure 7
Plot of cupping artifact through center of steel cylinder showing non-linearity correction. Left: uncorrected, right: corrected

Figure 8
Fuselage fragment. Top: uncorrected, bottom: corrected

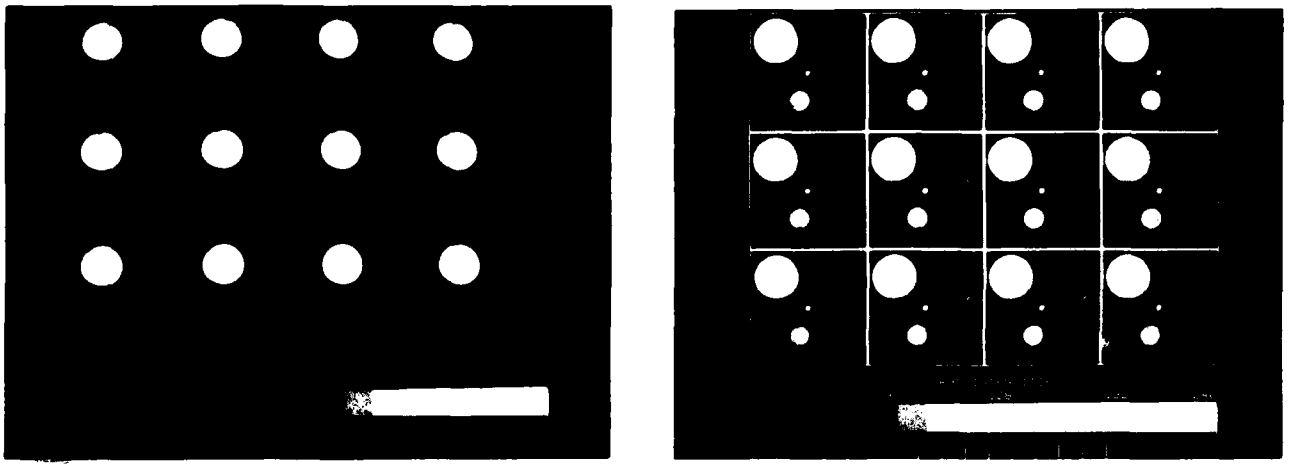

Figure 9
Neutron Tomograms of cylinders. Spacing is 1 mm between tomograms. Details shown for steel (left) and aluminum (right).

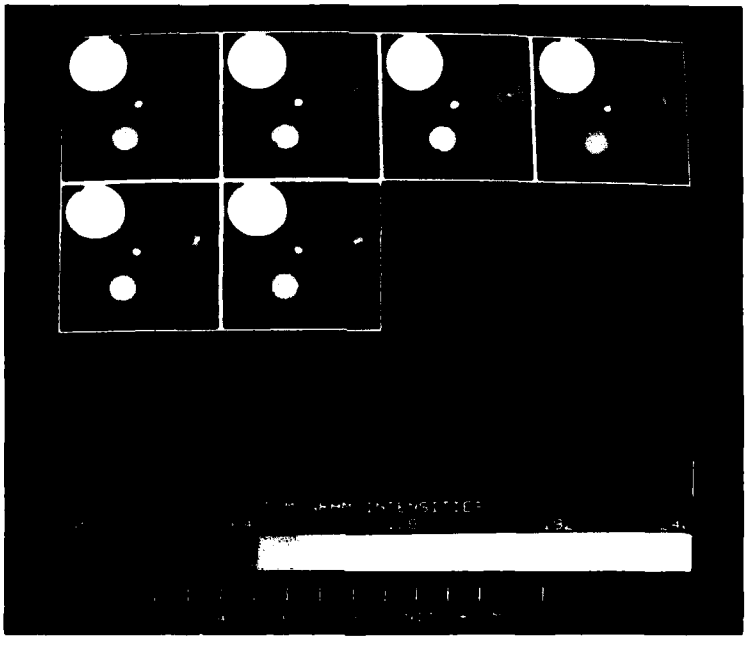

Figure 10
X-ray Tomograms of cylinders. Spacing is 2 mm between tomograms

Figure 11
Comparison of neutron and x-ray tomograms for fuselage part

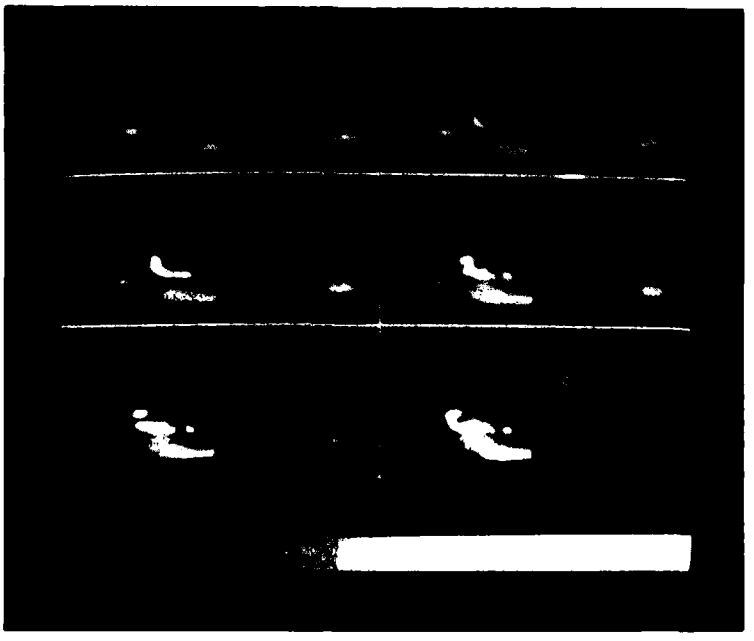

Figure 12
Figs. 12 through 14 show 16 neutron tomograms at 1 mm intervals

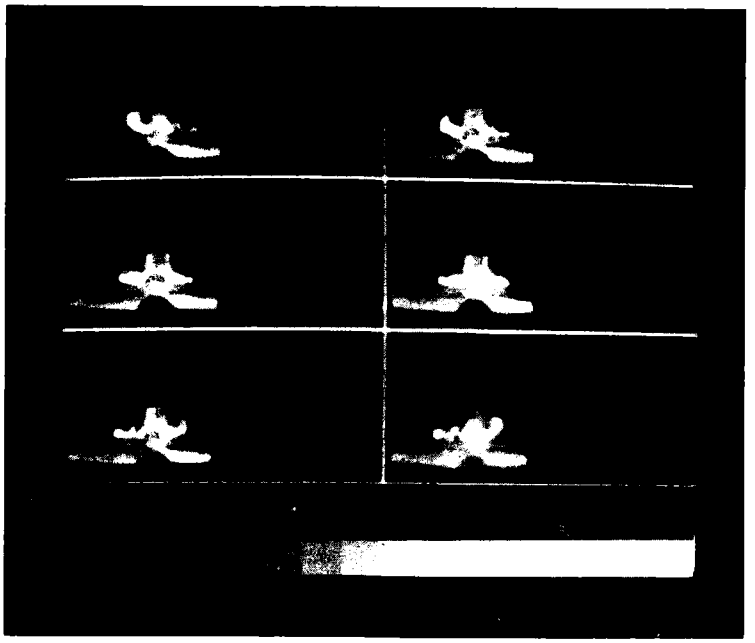

Figure 13
See caption for Fig.12

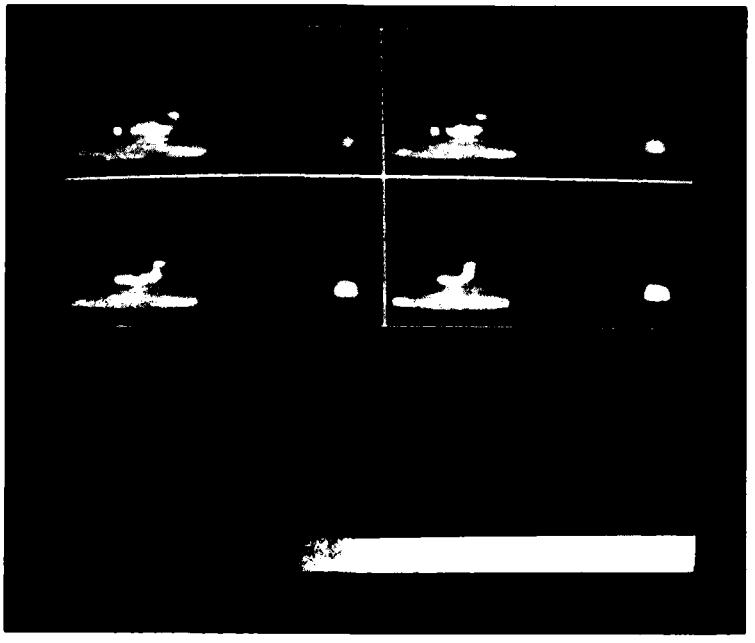

Figure 14
See caption for Fig.12

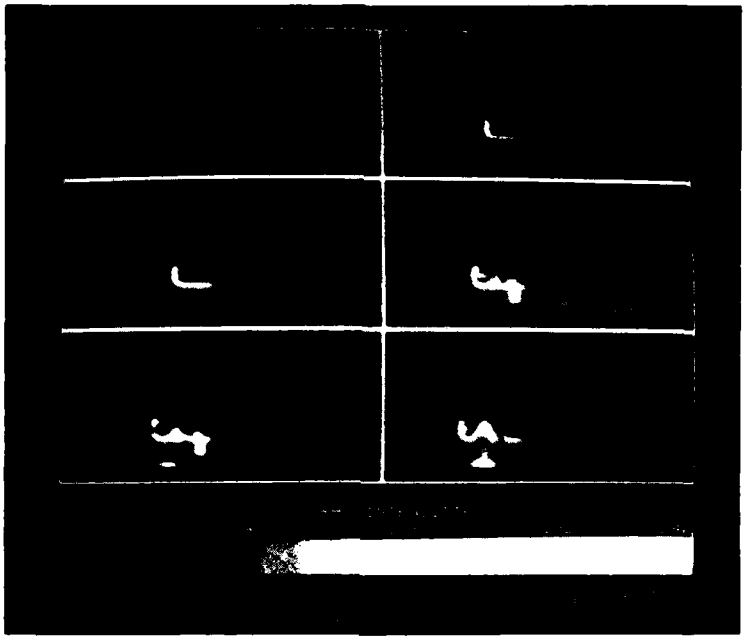

Figure 15
Figs. 15 through 17 show 16 x-ray tomograms at 1 mm intervals

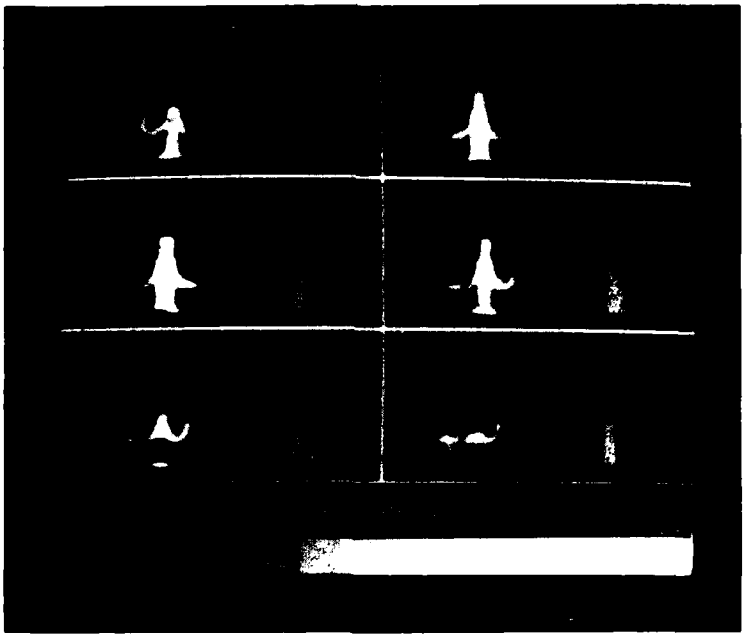

Figure 16
See caption for Fig.15

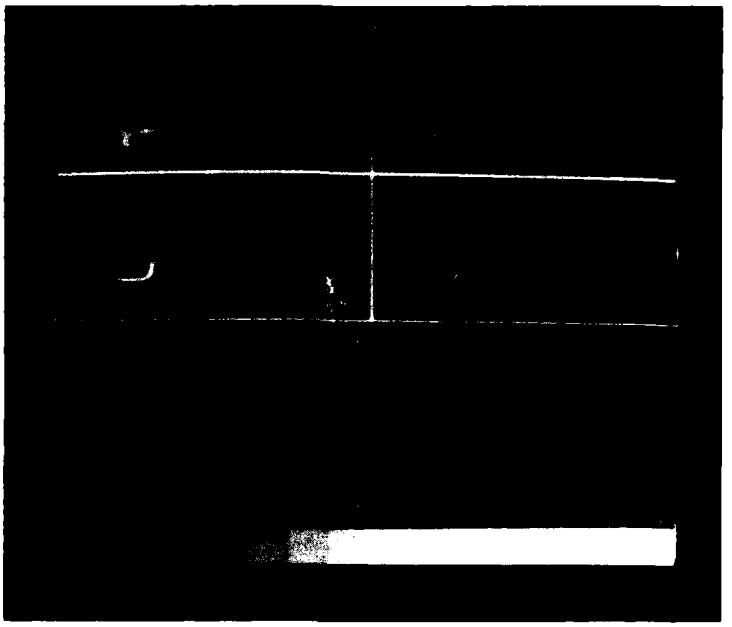

Figure 17
See caption for Fig.15

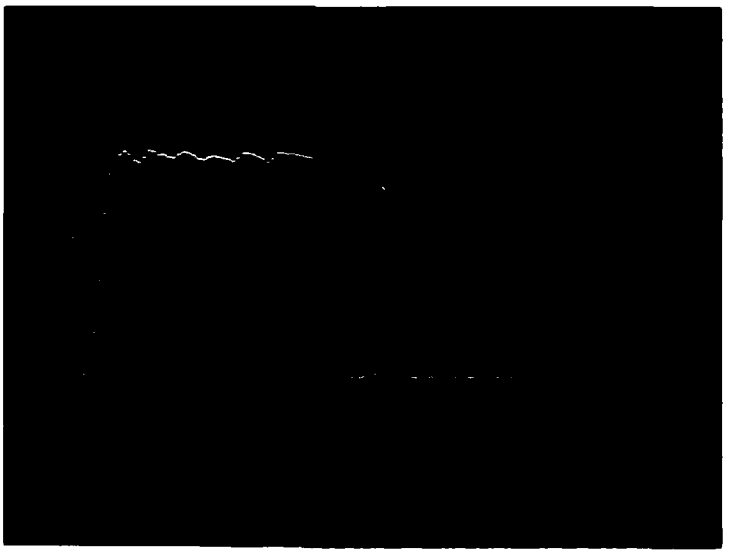

Figure 18
Estimate of x-ray linear attenuation coefficient vs. distance across a diameter of the steel cylinder

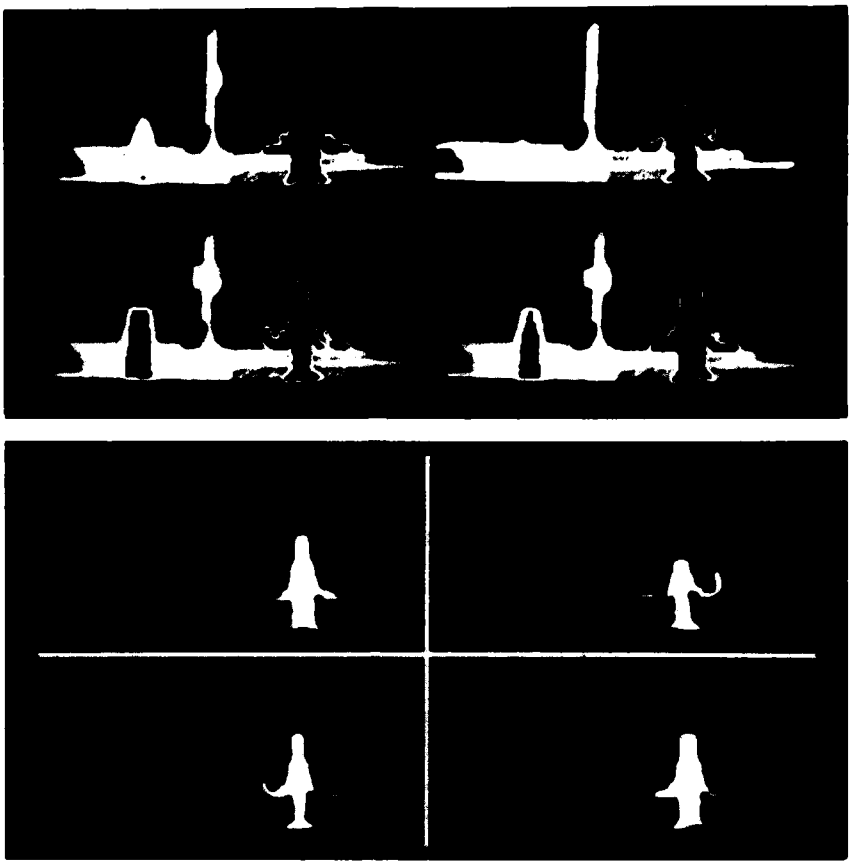

Figure 19
X-ray tomogram with intensity windows centered on aluminum (top) and steel (bottom).

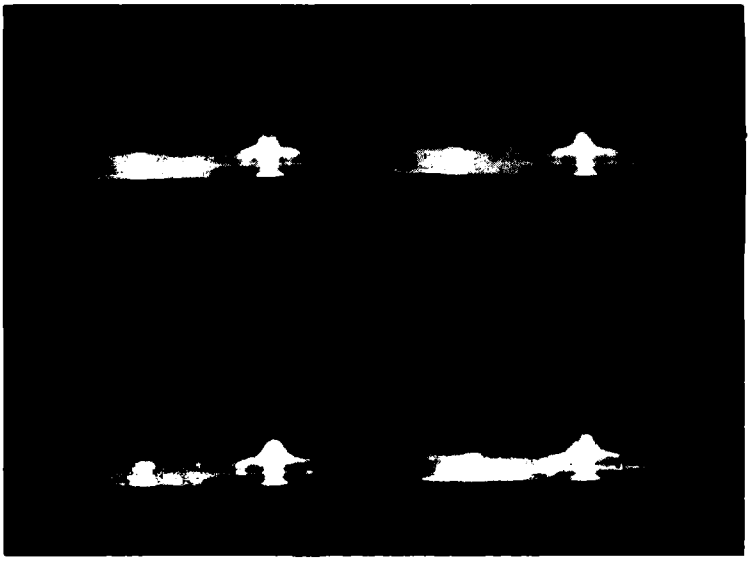

Figure 20
Additive reprojections of x-ray tomograms.
Sequence is left to right,top to bottom.

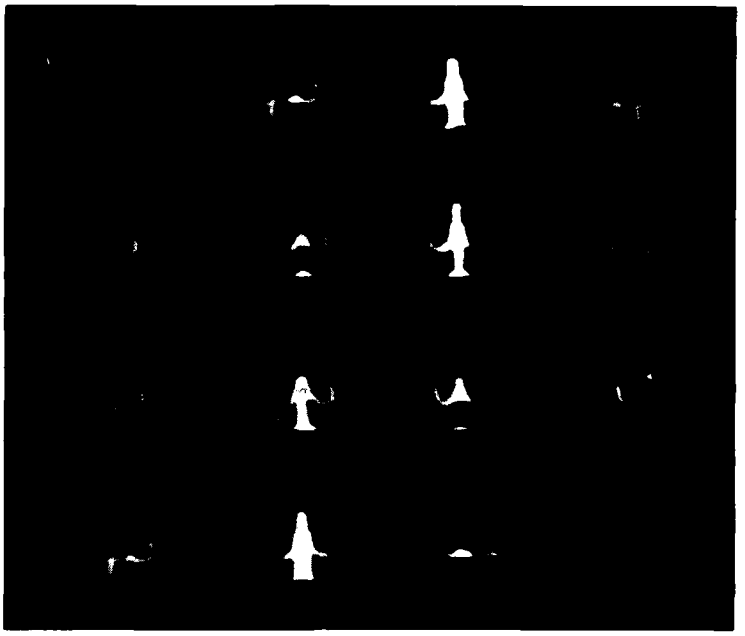

Figure 21
X-ray tomograms with all materials but fastener set to zero.

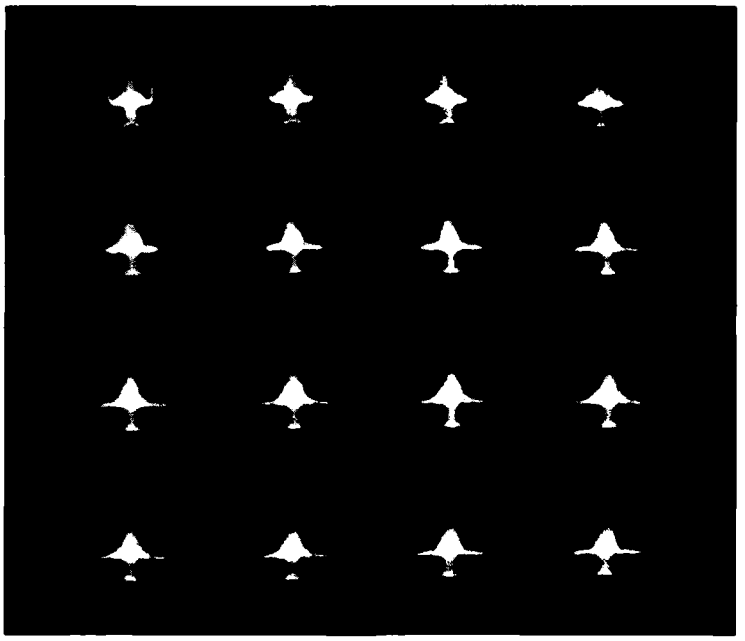

Figure 22
High-contrast reprojections in the sequence of Fig.20.

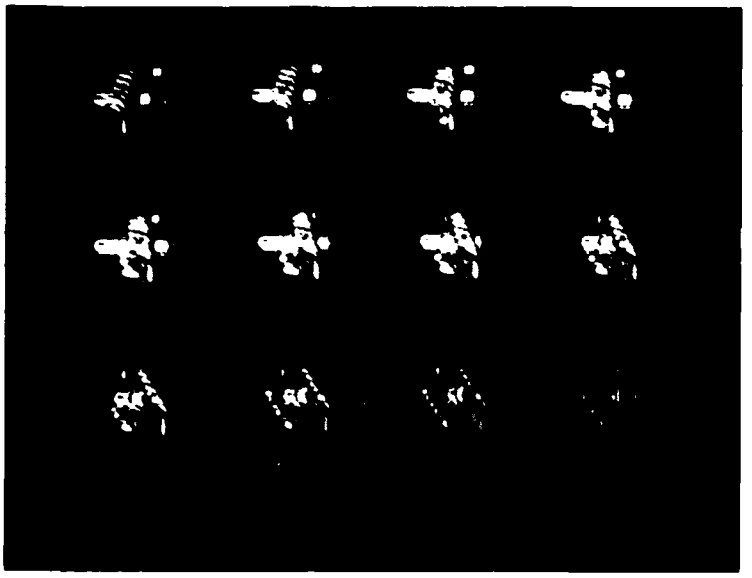

Figure 23
X-ray tomogram reprojection using the source-attenuation model

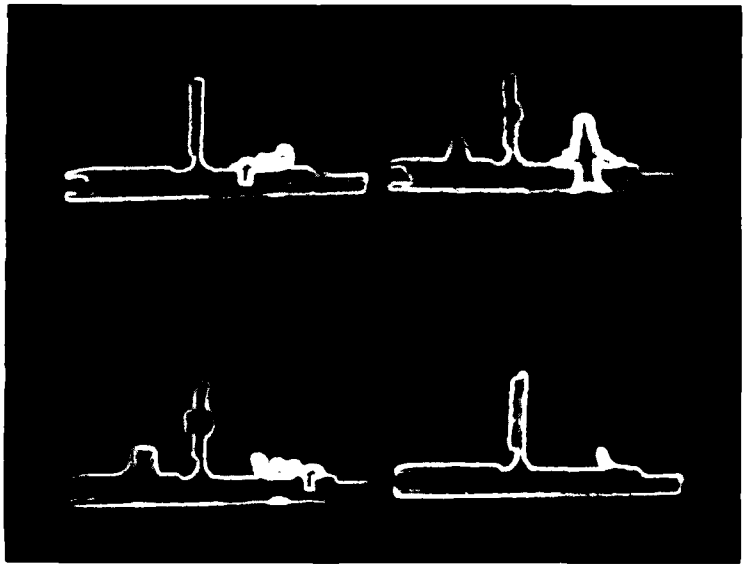

Figure 24
The Sobel operator applied to 4 x-ray tomograms of the fuselage

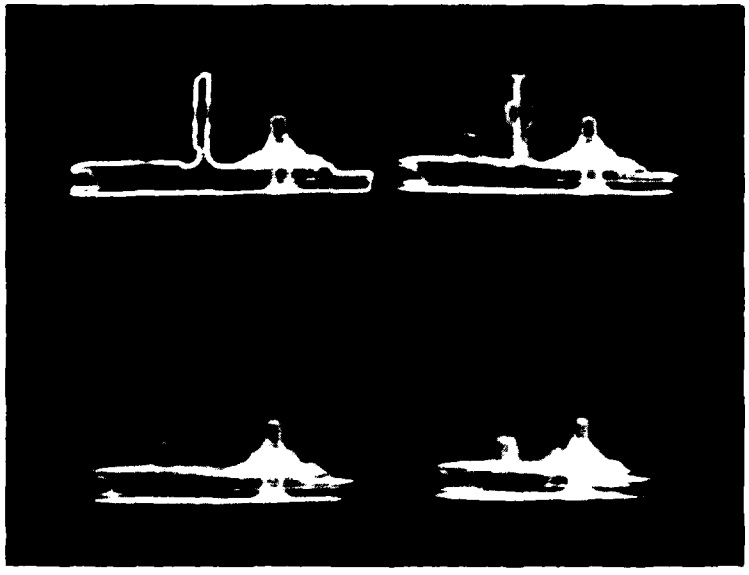

Figure 25
Additive reprojections of the Sobel-operated fuselage tomograms

REFERENCES

Barton,C.F., private communication, 1983.

Barton,C.F., Trans.Am.Nucl.Soc. v.27 (1977) pp 212-213.

Bracewell,R.N., J.Comp. Assisted Tomog. v.1 (1977) pp 6-15.

DeVolpi,A. private communication, 1983.

DeVolpi,A., and Rhodes,E.A., Materials Evaluation, v.40 (1982) pp 1273-1279.

Duerinckx,A.J., Image Statistics and Nonlinear Artifacts in Computed Transmission X-ray Tomography Ph.D. Thesis, Dept. of Elec.Engg., Stanford Univ., 1979

Dutta,K., Jaffey,S.M., Proceedings of the 1983 Array Conference of Array, the FPS Array Processor user society (April 1983) pp 2-9.

Herman,G.T., Image Reconstruction from Projections, Academic Press, 1980.

Hopkins,F.F., Morgan,I.L., Ellinger,H.D., Klinkseik,R.V., Meyer,G.A., and Thompson,J.N., IEEE Tr.Nuc.Sc. v.NS-28 (1981) pp 1717-1720.

Huesman,R.H., Gullberg,G.T., Greenberg,W.L., and Budinger,T.F., Donner Algorithms for Reconstruction Tomography Univ. of Calif., Berkeley, 1977.

Jaffey,S.M. and Dutta,K., SPIE v.367 Processing and Display of Three-Dimensional Data (1982), pp 130-140.

Joseph,P.M., and Spital,R.D., Med.Phys., v.9 (1982) pp 464-472.

Joseph,P.M., and Schulz,R.A., Med.Phys. v.7 (1980) pp 692-702.

Joseph,P.M., Spital,R.D., and Stockham,C.D., Comput. Tomog., v.4 (1980) pp 189-206.

Koeppe,R.A., Brugger,R.M., Schlapper,G.A., Larsen,G.N., and Jost,R.J., J.Comp. Assisted Tomog. v.5 (1981) pp 79-88.

Macovski,A., private communication, 1983.

Macovski,A., Medical Imaging Systems, Prentice-Hall, 1983.

Newacheck,R.L., of Aerotest Operations, private communication, 1983.

Richards,W.J., McClellan,G.C., and Tow,D.M., Materials Evaluation, v.40 (1982) pp 1263-1267.

Robb,R.A., private communication, 1983.

Schlapper,G.A., Larsen,G.N., Koeppe,R.M., Jost,R.A., and Brugger,R.M., Trans.Am.Nucl.Soc. v.34 (1980) pp 176-178.

Stonestrom,J.P., Non-linearities in X-ray Computerized Tomographic Imaging Systems Ph.D. Thesis, Dept. of Elec. Engg., Stanford Univ. 1976.

Stonestrom,J.P., Alvarez,R.E., and Macovski,A., IEEE Tr.Biomed.Engg., v.BME-28 (1981) pp 128-141.

Tyufakov,N.D., and Shtan,A.S., Principles of Neutron Radiography Amerind Publishing Co. Ltd., New Delhi (1979).

Verly,J.G., and Bracewell,R.N., J.Comp. Assisted Tomog., v.3 (1979) pp 662-678.